Experimental verification of multirate and Model Predictive Control for discrete-valued control systems

Nijihiko ISHIHARA*, Yuichi CHIDA* and Masaya TANEMURA*

* Department of Mechanical Systems Engineering
4-17-1 Wakasato, Nagano-shi, Nagano, 380-8553, Japan
E-mail: chida@shinshu-u.ac.jp

Abstract

A plant with discrete-valued control is considered in this study. In discrete-valued control systems, the control input resolution, which is determined by the minimum value of the amplitude of the discrete-valued input and period, directly affects the control performance. If insufficiently short periods are specified, the control performance decreases due to the poor resolution of the discrete-valued input. To overcome such decrease, multirate control, which employs individual periods for output measurement and control input switching, was adopted in this study. We analyzed a decrease in the discrete-valued control performance caused by the poor control input resolution in pneumatic isolation table control, and numerical simulations and experiments showed that the use of multirate control is effective despite a long output period. The multirate control input was determined based on the Model Predictive Control, and a Kalman filter was employed in the experiments to reduce sensor noise for the pressure sensors.

Keywords : Discrete actuators, Discrete-valued control, Multirate control, Model Predictive Control, Quantized signals, Pneumatic isolation table

1. Introduction

Currently, research on discrete-valued control systems, including discrete actuators, has attracted significant interest owing to their merits, such as low cost of the device configuration and easy manageability, compared with continuous input systems. Various studies on discrete-valued control systems have been reported, including those on temperature control (Dostal and Ferkl, 2014), tracking control (Mitsuhashi et al., 2019), and vibration control (Chida et al., 2019; Koike and Chida, 2012; Koike et al., 2013; Maruyama et al., 2013; Maruyama et al., 2015). Compared with the continuous system, it is quite difficult to control the systems, which is attributed to the restricted valued input. Consequently, some methods have been proposed for discrete-valued control systems, which are based on the Lyapunov function (Koike and Chida, 2012; Koike et al., 2013), optimal dynamic quantizer (Azuma and Sugie, 2007; Azuma and Sugie, 2008; Minami et al., 2007), feedback modulator (Ishikawa et al., 2007), and pulse-width-modulation scheme (Suzuki and Hirata, 2015).

In discrete-valued control systems, the control input resolution directly affects the control performance, and it is determined by the minimum value of the discrete-valued input amplitude and period. The minimum amplitude of inputs is restricted by actuators mounted in the plant. In contrast, the input period is sometimes required to be specified as sufficiently short to realize a sufficient control performance. However, there are some situations where sufficiently short output periods cannot be specified because of the restriction of the frequency range of sensors. In such cases, the control performance decreases to coincide with the output period restriction if the input period is long. To overcome such a decrease, multirate control, which employs individual periods for output measurement and control input switching, is effective (Berg, 1988; Fujimoto, 2009), and we can obtain sufficient control performance using shorter input periods than the output. In this study, we analyze the decrease in performance caused by long output periods in a pneumatic isolation table control and verify that the multirate control for plants whose output period is restricted relatively long is effective.
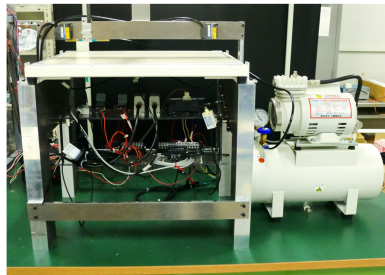
Fig. 1   Experimental device for the pneumatic isolation table. The device consists of the table, air springs, four solenoid on-off valves, buffer tanks, pressure sensors, displacement sensors, a main tank, and transmission pipes.
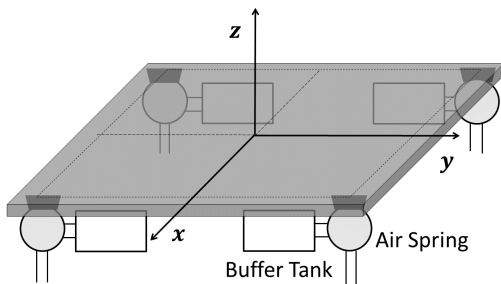

Fig. 2   Table model for the vertical motion. Four springs move in synchronization in vertical direction. Internal pressure varies depending on the mass flow of the air through the buffer tanks and the main tank.
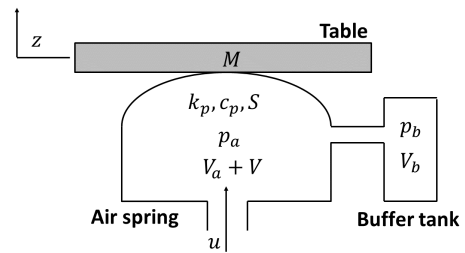

Fig. 3   Air spring model. The table is supported by the air spring, and the internal pressure of the spring is controlled by the mass flow through the main tank.
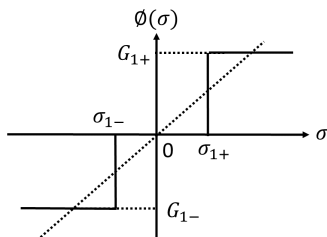

Fig. 4   Quantizer. The continuous signal σ is discretized by $\phi(\sigma)$.
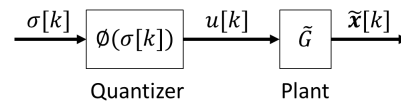

Fig. 5   Block diagram of the plant. The plant includes a linear model $\tilde{G}$ and the quantizer.

Here, the multirate control input was determined based on the MPC-based method proposed in (Chida et al., 2019). Chida et al. (2019) performed simulation verification for the pneumatic isolation table, but experimental verification has not been reported. In this study, experimental verification was performed using the method proposed in (Chida et al., 2019), and the control performance was evaluated for the pneumatic isolation table. In (Chida et al., 2019), the Padé approximation was used to evaluate the time delay in a system. However, in this study, we derived the control law without assuming the Padé approximation. In addition, there is a need to reduce noise in the pressure sensors built in the plant, which we achieved using a Kalman filter.

This paper is structured as follows: the discretized plant and configuration of a pneumatic isolation table are introduced in Section 2; the problem presentation is discussed in Section 3; the outline of the proposed method is presented in Section 4; the control system design and the numerical results are presented in Section 5; the main experimental results are discussed in Section 6; Section 7 presents the conclusions.

2. Plant

In this study, an experimental device for a pneumatic isolation table system was employed to analyze the discrete-valued control and determine the effect of introducing the multirate control. The plant is a pneumatic isolation table system, as shown in Fig. 1. The table is supported by four air springs, and a sketch of the air springs is shown in

Fig. 2. Each spring is connected to a buffer tank. We focused on the vertical translational motion, which is controlled by changing the inner pressure of the air springs. Thus, the model of the spring is indicated as Fig. 3, where it is assumed that an equivalent spring is used. The internal pressure of the springs is controlled by varying the mass flow rate through the air pipes. The vertical displacement of the table z is measured using a displacement sensor. The velocity $\dot{z}$ is obtained by online derivation calculation. Additionally, p_a and p_b, which denote the deviation of the internal pressure of the spring and buffer tank from the equilibrium p_0, respectively, are measured by pressure sensors. Here, we assumed that the inner pressure of the four air springs corresponds to identical values, p_a, and that of the buffer tanks corresponds to a common value, p_b. The system includes a time delay of $L = 20$ [ms], which includes input delay through air transmission, 10 [ms], and the calculation time delay for the control input calculation. The parameters of the model are described in (Chida et al., 2019), and the state space equation is expressed as follows:

$$\dot{x}(t) = A_c x(t) + B_c u(t - L). \tag{1}$$

The plant G is obtained by discretizing Eq. (1), assuming that the zero-order hold is used with the input and output period T_s as follows:

$$G : x[k + 1] = Ax[k] + Bu[k - d], \tag{2}$$

where $k \in \{0\} \cup \mathbb{N}_+$, $d \in \mathbb{N}_+$, $x \in \mathbb{R}^{N \times 1}$, and $u \in \mathbb{R}$ denote the step number of the discrete system, step number of the time delay, state variable, and control input, respectively. It is defined as the state variable $x[k] = [z[k], \dot{z}[k], p_a[k], p_b[k]]^T$, and $N = 4$ is introduced. To improve the overall outlook of the control system design, the past control input of the time delay is considered a part of the state variables. Then, G can be extended to $\tilde{G}$ in Eq. (3), where $\tilde{x}$, $\tilde{A}$, and $\tilde{B}$ are denoted as follows:

$$\tilde{G} : \tilde{x}[k + 1] = \tilde{A}\tilde{x}[k] + \tilde{B}u[k], \tag{3}$$

$$\tilde{x}[k] = [x[k]^T, u[k - d], u[k - d - 1], \ldots, u[k - 1]]^T, \tag{4}$$

$$\tilde{A} = \left[\begin{array}{cc|c} A & B & 0_{N \times (d-1)} \\ \hline & & I_{(d-1) \times (d-1)} \\ 0_{d \times (N+1)} & & 0_{1 \times (d-1)} \end{array} \right], \quad \tilde{B} = \left[\begin{array}{c} 0_{(N+d-1) \times 1} \\ 1 \end{array} \right].$$

It is assumed that $(\tilde{A}, \tilde{B})$ is controllable and $\tilde{x}$ is measurable. The control input is added to the plant through a quantizer $\phi \colon \mathbb{R} \to \mathbb{R}$, which changes the continuous input signal $\sigma[k]$ to a discretized signal $u[k] = \phi(\sigma[k])$ as follows:

$$u[k] = \phi(\sigma[k]), \tag{5}$$

where ϕ satisfies $\phi(0) = 0$. It is assumed that the input consists of three discrete values, namely, G_{1+}, 0, and G_{1-}, where $G_{1+} = 2.70 \times 10^{-4}$ [kg/s] and $G_{1-} = -2.57 \times 10^{-4}$ [kg/s]. Thereafter, the quantizer ϕ provides the following admissible three-valued input.

$$\phi(\sigma) = \begin{cases} G_{1+} & , \ if & \sigma_{1+} \leq \sigma, \\ G_{1-} & , \ if & \sigma \leq \sigma_{1-}, \\ 0 & , \ others, \end{cases} \tag{6}$$

where $\sigma[k]$ denotes the input of ϕ, and σ_{1+} and σ_{1-} denote the design parameters. The parameters are specified as $\sigma_{1+} = G_{1+}/2$ and $\sigma_{1-} = G_{1-}/2$. The quantizer is shown in Fig. 4, and a block diagram is shown in Fig. 5.

3. Issues on the discrete-valued control

In this section, an example of performance deterioration, which is the vibration suppression of the pneumatic isolation table, is discussed when a long period is set for the input as well as output period. First, the difference in the response is confirmed when a step-type input is applied to the plant in one input period, T_u. Figures 6 and 7 show the responses of the displacement with $T_u = 5$ [ms] and $T_u = 20$ [ms] as input periods, respectively, when the input $G_{1+} = 2.70 \cdot 10^{-4}$ [kg/s] is set as the step-type control amplitude for one input period. The maximum value of the vibration response and steady-state in Fig. 7 are approximately four times as high as that in Fig. 6. The values correspond to the input amplitude that the applied input in Fig. 6 is $G_{1+} \cdot 0.005 = 1.35 \cdot 10^{-6}$, whereas the input in Fig. 7 is $5.4 \cdot 10^{-6}$, which is four times as large as that
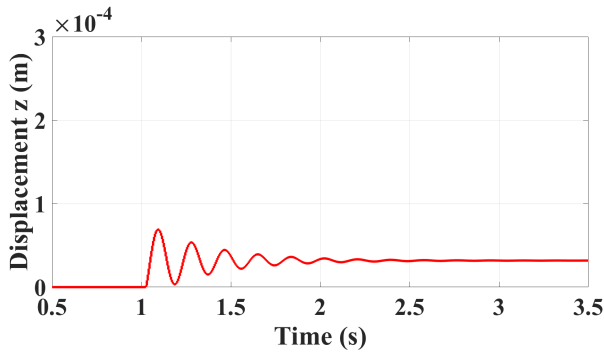
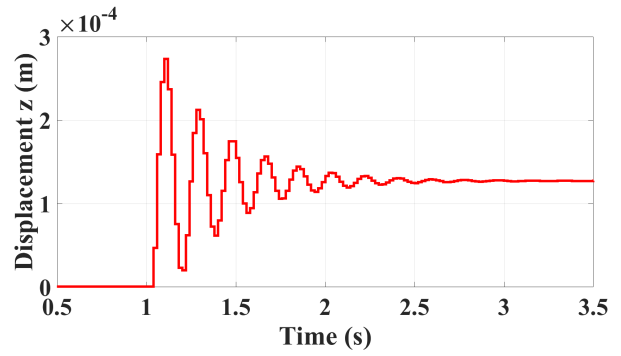Fig. 6 Step response with $T_u = 5$ [ms] input period. The amplitude and the steady-state value depends on T_u.

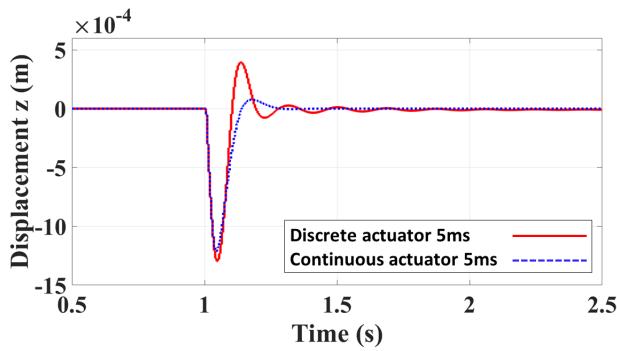Fig. 7 Step response with $T_u = 20$ [ms] input period. The amplitude and steady-state value depend on T_u.

Fig. 8 Control responses with respect to control with $T_u = T_y = 5$[ms] period. Sufficient damping performance is obtained.
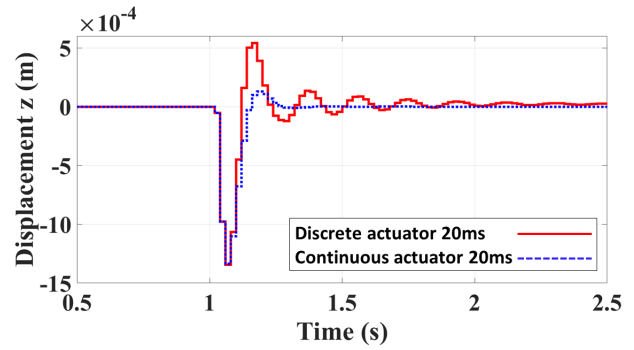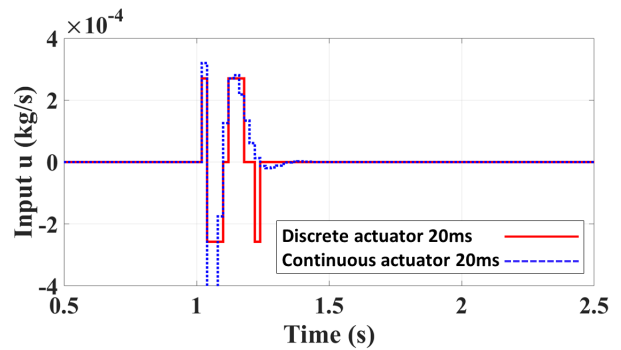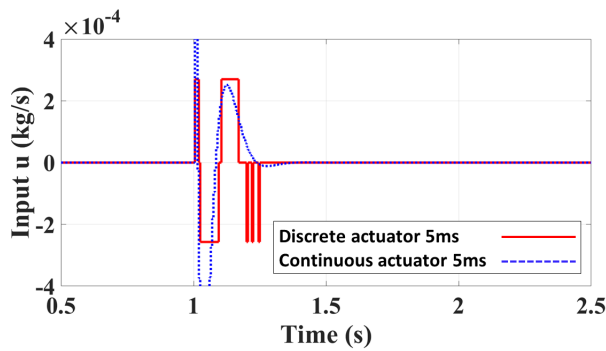

Fig. 9 Control responses with respect to control with $T_u = T_y = 20$[ms] period. Damping performance is deteriorated compared to the case of $T_u = T_y = 5$[ms].

in Fig. 6. This response implies that the feasible magnitude to attenuate a vibration by the control is probably restricted by the specified input period, T_u. Furthermore, the convergence time in Fig. 6 is shorter than the time in Fig.7. For the above reason, it is necessary to decide the input and output period appropriately for successive damping control. Following that, the simulation results with feedback control of vibration suppression under the condition that the input and output periods are the same are shown in Figs. 8 and 9, and the period are 5 [ms] and 20 [ms], respectively. The figures are obtained using the conventional method for "Discrete actuator" shown in Section 5.1. The design parameters are shown in Section 5.1 for the case where the period is 20 [ms]. For the case where the period is 5 [ms], some parameters and the feedback gains are different from that of 20 [ms] period because the dimension of the state vector for the time delay of the plant is different. The "Continuous actuator" indicates the responses under the same conditions of the "Discrete actuator", except that $\phi(\sigma) = \sigma$. Figures 8 and 9 express the response of the displacement of the table and control input, respectively. They show that the control performance is decreased when the period is long. This is caused by the minimum resolution power of the control input, which is determined by T_u and G_{1+}, as shown in Figs. 6 and 7. To overcome the issue, it is effective to use pulses of short duration for the control input, and the multirate input control is suitable for the purpose. By the multirate control, it is possible to specify the input period independently with the output period, so that we can use smaller resolving power of the control input. In that case, the control input determination algorithm and implementation

of the algorithm for real applications are important. The control algorithm is proposed in Section 4, and the issue of the implementation is demonstrated in Section 5 and 6.

4. Proposed control method

The algorithm of the control method with the discrete-valued control input is proposed in (Chida et al., 2019) based on (Maruyama et al., 2013; Maruyama et al., 2015). A block diagram of the multirate control system is shown in Fig. 10. The output period of $\tilde{x}[k]$ is T_y, and the input period is T_u. We assume that $T_y > T_u$, $n = T_y/T_u$, and n corresponds to a positive integer, and k represents the step number for inputs. The relationship between the input and output is shown in Fig. 11. In Fig. 11, i indicates the step number for the output. The output is measured when k is the multiple of n, and k' indicates the input step number synchronized with the output step number, i. Then, it is assumed that n can be divided evenly into k', so k' is described as $k' \in \{k \in I \mid n|k\}$, where $I := \mathbb{N} \cup \{0\}$ and $\mathbb{N}$ is the sets of positive integers. For $i \in \{i \in I \mid i = k'/n\}$, the control input $U[i]$ is defined as follows:

$$U[i] := [u[k'], u[k' + 1], \cdots, u[k' + n - 1]]^T. \tag{7}$$

State variable is defined as $\tilde{x}_m[i] := \tilde{x}[k']$ which corresponds to the output period. Then, the state space equation for i is described as follows using Eq. (3),

$$
\begin{aligned}
\tilde{x}_m[i + 1] &= \tilde{x}[k' + n] \\
&= \tilde{A}^n \tilde{x}[k'] + \tilde{A}^{n-1}\tilde{B}u[k'] + \tilde{A}^{n-2}\tilde{B}u[k' + 1] + \cdots + \tilde{B}u[k' + n - 1] \\
&= A_m \tilde{x}_m[i] + B_m U[i], \\
A_m &:= \tilde{A}^n \ , \ B_m := [\tilde{A}^{n-1}\tilde{B}, \tilde{A}^{n-2}\tilde{B}, \cdots, \tilde{B}].
\end{aligned} \tag{8}
$$

Here, the method for determining the control input $U[i]$ with measurement $\tilde{x}_m[i]$ is a problem. Thus, the MPC method is applied. A positive quadratic cost function is expressed as follows:

$$V[i] = \tilde{x}_m^T[i]P\tilde{x}_m[i], \tag{9}$$

where $P > 0$ denotes a solution of the Lyapunov equation in discrete time systems as follows:

$$(\tilde{A} - \tilde{B}F)^T P(\tilde{A} - \tilde{B}F) - P = -Q_L. \tag{10}$$

where F denotes a feedback gain such that $\tilde{A} - \tilde{B}F$ becomes the Schur stable matrix, and Q_L represents a specified arbitrary positive definite matrix. $V[i + 1]$ is obtained by substituting Eq. (8) for Eq. (9) as follows:

$$
\begin{aligned}
V[i + 1] &= \tilde{x}_m^T[i + 1]P\tilde{x}_m[i + 1] \\
&= (A_m \tilde{x}_m[i] + B_m U[i])^T P(A_m \tilde{x}_m[i] + B_m U[i]) \\
&= \tilde{x}_m^T[i]A_m^T P A_m \tilde{x}_m[i] + 2\tilde{x}_m^T[i]A_m^T P B_m U[i] + U^T[i]B_m^T P B_m U[i],
\end{aligned} \tag{11}
$$

where the first term in Eq. (11) is independent of the control input because we focus on the second and third terms. The cost function is reintroduced as a renewed cost function as follows based on (Maruyama et al., 2013; Maruyama et al., 2015):

$$
\begin{aligned}
J(U[i]) &= 2\tilde{x}_m^T[i]YU[i] + U^T[i]XU[i], \\
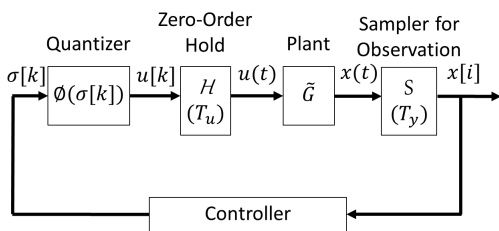X &:= B_m^T P B_m, Y := A_m^T P B_m.
\end{aligned} \tag{12}
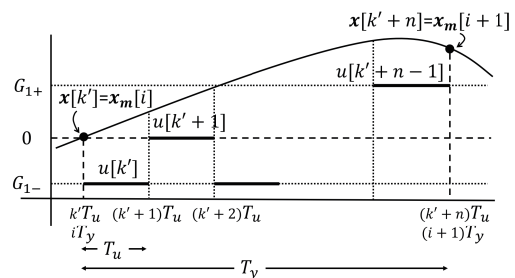$$

Fig. 10　Block diagram of the multirate control system

Fig. 11　Relationship between input and output periods for the multirate control

If it is assumed that n is not greater than N, $\boldsymbol{B}_m$ is column full rank and $\boldsymbol{X}$ is a positive definite matrix since $\boldsymbol{P} > 0$. The cost function is convex for $\boldsymbol{U}[i]$. The gradient and Hessian of $J(\boldsymbol{U}[i])$ are expressed as

$$\frac{\partial J}{\partial \boldsymbol{U}} = 2\boldsymbol{Y}^T \tilde{\boldsymbol{x}}_m^T[i] + 2\boldsymbol{X}\boldsymbol{U}[i], \tag{13}$$

$$\frac{\partial^2 J}{\partial \boldsymbol{U}^2} = 2\boldsymbol{X}. \tag{14}$$

The Hessian of Eq. (14) is a positive definite matrix because of $\boldsymbol{X} > 0$. Therefore, the cost function is convex. Here, we adopted a method that employs the gradient of the cost function proposed by (Maruyama et al., 2013; Maruyama et al., 2015) to solve the MPC control problem. The obtained input sequence $\boldsymbol{U}_{opt}$ is a candidate for $\boldsymbol{U}[i]$, and the following additional branch condition is used here.

$$\begin{cases} \boldsymbol{U}[i] = \boldsymbol{U}_{opt} & , \quad \text{if} \quad J(\boldsymbol{U}_{opt}) \le 0 \ \text{and} \ \Delta V[i] < 0, \\ \boldsymbol{U}[i] = 0 & , \quad \text{otherwise}, \end{cases} \tag{15}$$

Here, $\Delta V[i]$ is defined as

$$\Delta V[i] = V[i + 1] - V[i]. \tag{16}$$

The condition that $\Delta V[i] < 0$ is added to satisfy the boundedness of the state variable $\tilde{\boldsymbol{x}}_m[i]$ using the result of (Koike and Chida, 2012; Koike et al., 2013). The algorithm of the MPC method is summarized in Fig. 12, and the outline of the calculation procedure for each i is explained as follows:

Step 1: Decide the initial searching points $\boldsymbol{U}^0$ in advance. In this study, $\boldsymbol{U}^0 = \boldsymbol{0}$ is specified.

Step 2: Compute $\frac{\partial J(\boldsymbol{U})}{\partial \boldsymbol{U}}$ for $\boldsymbol{U} = \boldsymbol{U}^l$ and determine $\boldsymbol{U}^{l+1}$ for each l by (Maruyama et al., 2013; Maruyama et al., 2015). If $\boldsymbol{U}^{l-1} = \boldsymbol{U}^{l+1}$, set $\boldsymbol{U}^l$ and $\boldsymbol{U}^{l+1}$ as candidates for $\boldsymbol{U}_{near}$.

Step 3: $\boldsymbol{U}_{near}$ is obtained from $\boldsymbol{U}_{near} = \arg \min_{j=l,l+1} J(\boldsymbol{U}^j)$.

Step 4: $j \in \{1, \cdots, n-1\}$ is specified such that one of $u[k' + j]$ in $\boldsymbol{U}_{near}$ is shifted from $\boldsymbol{U}_{near}$ to the direction where $\nabla J < 0$. The shifted input is indicated by $\boldsymbol{U}_{near \to \Delta u_j}$. $\boldsymbol{U}'_{near} = \arg \min_{j=1,\cdots,n-1} J(\boldsymbol{U}_{near \to \Delta u_j})$ is obtained, and the same procedure is repeated using updated $\boldsymbol{U}_{near} \leftarrow \boldsymbol{U}'_{near}$ until $J(\boldsymbol{U}_{near}) \le J(\boldsymbol{U}'_{near})$ is satisfied. $\boldsymbol{U}_{opt}$ is obtained such that $\boldsymbol{U}_{opt} = \boldsymbol{U}_{near}$ using the terminal input $\boldsymbol{U}_{near}$.

Step 5: $\boldsymbol{U}[i]$ is obtained such that $\boldsymbol{U}[i] = \boldsymbol{U}_{opt}$ or $\boldsymbol{U}[i] = 0$ according to the condition that $J(\boldsymbol{U}_{opt}) \le 0$ and $\Delta V[i] < 0$ is satisfied or not.

5. Application to the control of a pneumatic isolation table

5.1. Control system design

5.1.1. Conventional method The switching method proposed by (Koike and Chida, 2012; Koike et al., 2013) and single-rate control such that $T_s = T_u = T_y$ are considered as conventional methods. T_s is the period for the digital control in the usual sense and $T_s = 20$ [ms]. $\boldsymbol{A}_1$ and $\boldsymbol{B}_1$ in Eq. (2) are introduced by discretizing Eq. (1) with $T_s = 20$ [ms]. $d = 1$, is introduced in Eq. (3) since T_s and the time delay are the same (20 ms). Then, $\tilde{\boldsymbol{A}}_1$ and $\tilde{\boldsymbol{B}}_1$ in Eq. (3) are introduced as follows:

$$\tilde{\boldsymbol{A}}_1 = \begin{bmatrix} \boldsymbol{A}_1 & \boldsymbol{B}_1 \\ \boldsymbol{0}_{1\times5} \end{bmatrix}, \quad \tilde{\boldsymbol{B}}_1 = \begin{bmatrix} \boldsymbol{0}_{4\times1} \\ 1 \end{bmatrix}.$$

The state feedback gain $\boldsymbol{F}_1$ is obtained by solving LQ(Linear Quadratic) optimal control problem by assuming the following weighting matrices:

$$\begin{cases} \boldsymbol{Q} = \text{diag}(10^3, 4 \times 10^5, 9.5 \times 10^{-6}, 9.5 \times 10^{-6}, 10^7), \\ \boldsymbol{R} = 1. \end{cases} \tag{17}$$

$\boldsymbol{F}_1$ is obtained using MATLAB® is obtained as follows: $\boldsymbol{F}_1 = [-5.36 \times 10^{-1}, 6.59 \times 10^{-3}, 1.39 \times 10^{-8}, 2.96 \times 10^{-7}, 8.03 \times 10^{-1}]$. $\tilde{\boldsymbol{A}}_1 - \tilde{\boldsymbol{B}}_1 \boldsymbol{F}_1$ corresponds to the Schur stable matrix. The positive matrix $\boldsymbol{P}_1$ is obtained by solving the Lyapunov equation as follows:

$$(\tilde{\boldsymbol{A}}_1 - \tilde{\boldsymbol{B}}_1 \boldsymbol{F}_1)^T \boldsymbol{P}_1 (\tilde{\boldsymbol{A}}_1 - \tilde{\boldsymbol{B}}_1 \boldsymbol{F}_1) - \boldsymbol{P}_1 = -\boldsymbol{Q}_L, \tag{18}$$

assuming $\boldsymbol{Q}_L = \boldsymbol{I}_5$, and the control law Φ_1 is described as follows:

$$\Phi_1 : u[k] = \begin{cases} \phi(-\boldsymbol{F}_1 \tilde{\boldsymbol{x}}[k]) & , \quad \text{if} \ \Delta V_c[k] < 0, \\ 0 & , \quad \text{otherwise}, \end{cases} \tag{19}$$
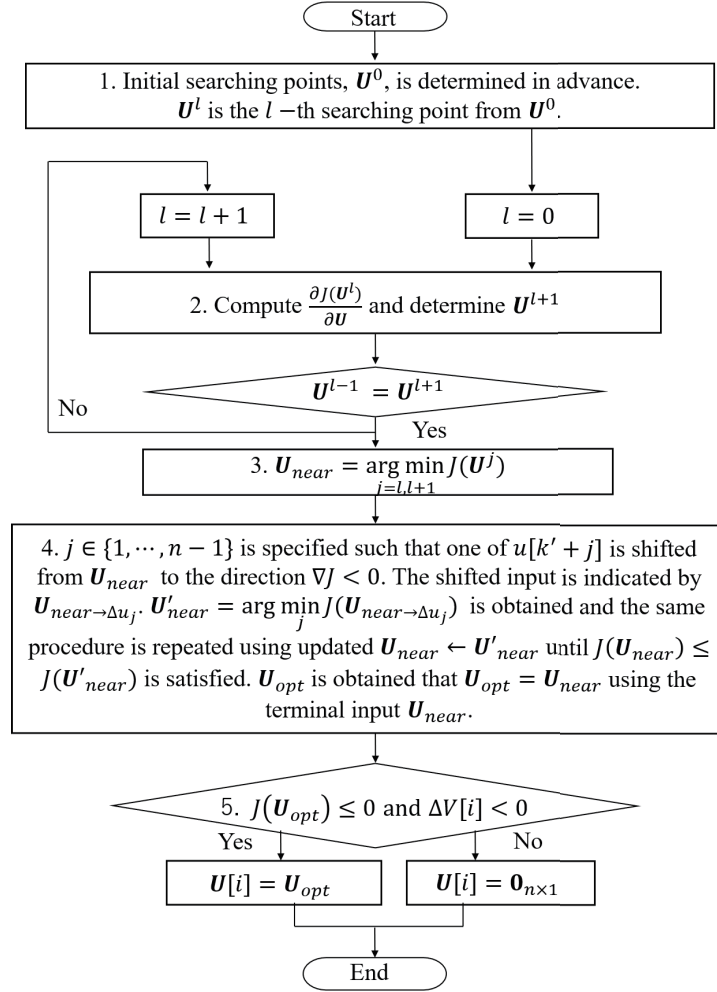
Fig. 12   Flow chart of calculation procedure to determine the optimal control input.

Additionally, $\Delta V_c[k]$ is defined as follows:

$$
\begin{aligned}
\Delta V_c[k] &= V[k+1] - V[k] \\
&= \tilde{x}^T[k+1]P_1\tilde{x}[k+1] - \tilde{x}^T[k]P_1\tilde{x}[k] \\
&= (\tilde{A}_1\tilde{x}[k] + \tilde{B}_1 u[k])^T P_1(\tilde{A}_1\tilde{x}[k] + \tilde{B}_1 u[k]) - \tilde{x}^T[k]P_1\tilde{x}[k].
\end{aligned}
\tag{20}
$$

5.1.2. Proposed method   We assumed that the output period is $T_y = 20$ [ms] and that for the input period is $T_u = 5$ [ms]. A_2 and B_2 in Eq. (2) are obtained by discretizing Eq. (1) with the period $T_s = 5$ [ms]. $n = T_y/T_u = 4$ and $d = 4$ in Eq. (3) are introduced. Then, $\tilde{A}_2$ and $\tilde{B}_2$ in Eq. (3) are introduced as follows:

$$
\tilde{A}_2 = \left[
\begin{array}{cc|c}
A_2 & B_2 & 0_{4\times3} \\
\hline
& & I_{3\times3} \\
0_{4\times5} & & 0_{1\times3}
\end{array}
\right], \quad
\tilde{B}_2 = \left[
\begin{array}{c}
0_{7\times1} \\
1
\end{array}
\right].
$$

The feedback gain F_2 described in (Chida et al., 2019) is designed by solving the LQ optimal control problem using MATLAB®, and the weightings are specified as follows:

$$
\begin{cases}
Q = \mathrm{diag}(10^9, 10^7, 5\times10^{-5}, 5\times10^{-5}, 10^7, 10^7, 10^7, 10^7), \\
R = 1.
\end{cases}
\tag{21}
$$

The obtained feedback gain was $F_2 = [-1.53, 6.14\times10^{-2}, 4.79\times10^{-8}, 7.02\times10^{-7}, 6.51\times10^{-1}, 6.32\times10^{-1}, 6.13\times10^{-1}, 5.81\times10^{-1}]$, and $\tilde{A}_2 - \tilde{B}_2 F_2$ corresponds to the Schur stable matrix. The positive matrix P_2 was obtained by solving the Lyapunov equation (10) with $Q_L = I_8$. It is appropriate to use the same parameters Q and R, for the conventional and proposed methods. However, it is impossible because the dimensions of the state variables of the conventional and

proposed plants are different. The first four variables, z, $\dot{z}$, p_a, and p_b, coincide in the two plants; thus proving that the first four parameters of $\boldsymbol{Q}$ are the same. Moreover, we could not obtain sufficient control performance using the same parameters for the conventional and proposed methods. Therefore, $\boldsymbol{Q}$ was retuned by trial-and-error to obtain sufficient performance using the conventional method.

5.2. Numerical simulations

Numerical simulations were performed on the pneumatic isolation table system model. The impulse disturbance responses were obtained for the proposed and conventional methods. The impulse disturbance corresponds to the disturbance generated by dropping a rubber baseball from a height of 600 [mm] above the isolation table. The disturbance is applied 1 [s] after starting the simulation. The obtained simulation results are shown in Fig. 13. The left figure shows the response of the displacement z, and the right figure shows the control inputs. In each figure, the solid blue line represents the response of the proposed method, and the dashed red line represents that of the conventional method. As shown in Fig. 13, the performance of the proposed method is superior to that of the conventional method. The key point in the proposed method is that it makes the resolution of the control input value finer by using a multirate control input. If the period is specified such that $T_s = T_y = T_u = 5$ [ms] in the conventional method, it is possible to obtain the responses as indicated by the solid line in Fig. 8. The response is similar to that of the proposed method, as shown in Fig. 13. This implies that we can consider a relatively long output period, although it is necessary to specify a relatively short input period in the case of a plant with a quantized input.

6. Experiments

6.1. Experimental system configuration

The configuration of the experimental device is depicted in Fig. 14. The data obtained from the laser-displacement and pressure sensors, which are attached to the experimental device, are converted by A/D(Analog/Digital) conversion, and the control input applied to the plant is determined by DSP(Digital Signal Processor) calculations. After deciding the control input, the voltage command is conveyed to the solenoid valve through digital input-output and D/A(Digital/Analog) conversions.

6.2. Observer

It is necessary to remove noise from the sensor signal because the signals from the pressure sensor are noisy. Thus, we designed a Kalman filter and performed experiments with the estimated values of the state $\hat{\boldsymbol{x}}$, which are expressed as follows:

$$\hat{\boldsymbol{x}}[k] = \boldsymbol{A}\hat{\boldsymbol{x}}[k-1] + \boldsymbol{B}u[k-d-1] + \boldsymbol{K}(\boldsymbol{y}[k] - \boldsymbol{C}\boldsymbol{A}\hat{\boldsymbol{x}}[k-1] - \boldsymbol{C}\boldsymbol{B}u[k-d-1]). \qquad (22)$$

Here, $\boldsymbol{A}$, $\boldsymbol{B}$ and $\boldsymbol{C}$ are the matrices of the state space equation in the discrete time of the plant and they are specified such that $\boldsymbol{A} = \boldsymbol{A}_1$ and $\boldsymbol{B} = \boldsymbol{B}_1$ for the conventional method and $\boldsymbol{A} = \boldsymbol{A}_2$ and $\boldsymbol{B} = \boldsymbol{B}_2$ for the proposed method. $\boldsymbol{C} = \boldsymbol{I}$ is employed in each case. A block diagram of Eq. (22) is shown in Fig. 15, where $\boldsymbol{C} = \boldsymbol{I}_4$, $\boldsymbol{y} = \boldsymbol{x}$, and $\boldsymbol{K}$ are the output matrix, measured values, and Kalman gain, respectively. The Kalman gain $\boldsymbol{K}$ is introduced to Eq. (23) and positive
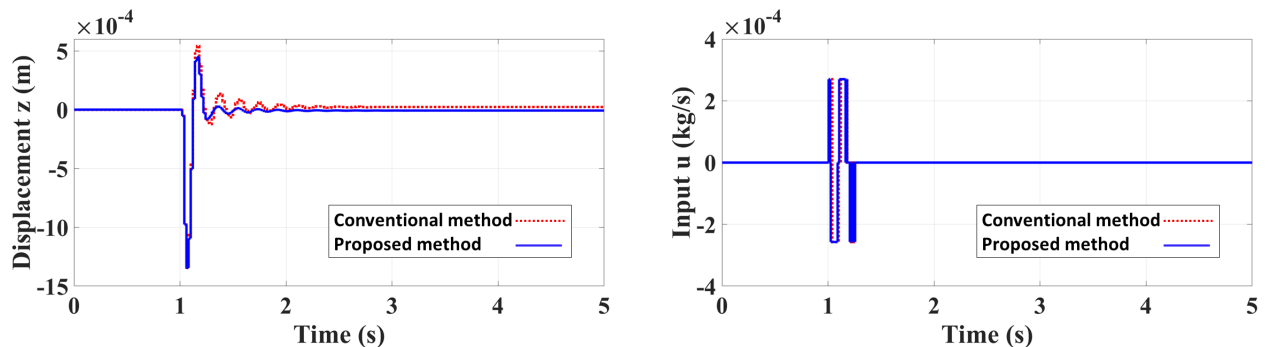

Fig. 13   Simulation results for impulse disturbance response. The proposed method provides superior control performance to the conventional method.
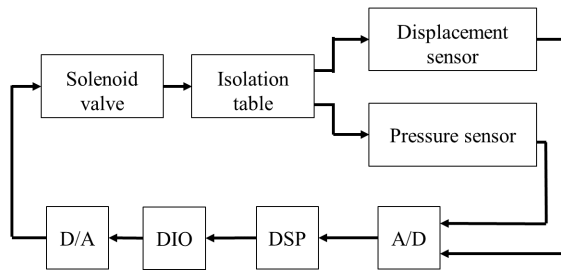
Fig. 14 Control system in experiment. Multirate and MPC control calculation is executed by DSP by using a displacement sensor and pressure sensor signal.
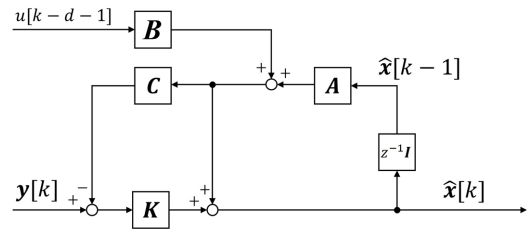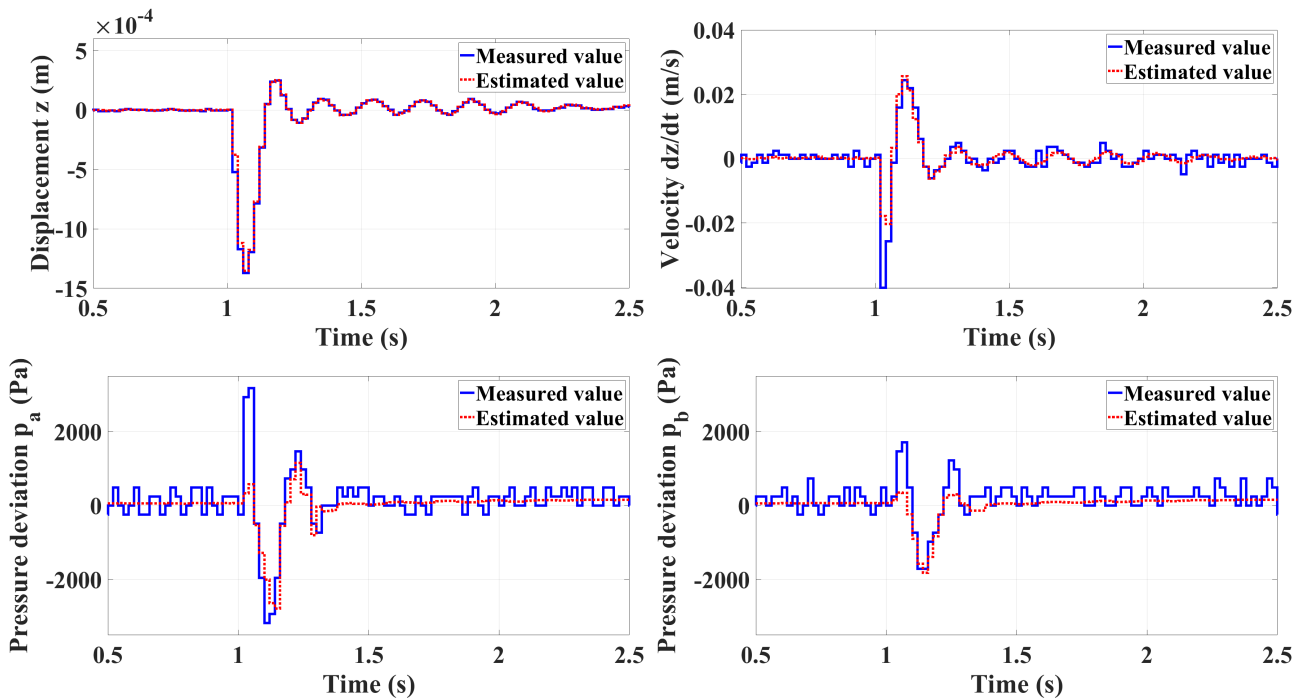
Fig. 15 Block diagram of Kalman filter

Fig. 16 Measured and estimated values using the Kalman filter for an impulse-type disturbance control response. The disturbance is applied at 1 [s]. Each variable is estimated accurately by reducing noise.

definite symmetric matrix is P introduced to Eq. (24), which is the Riccati equation in discrete time systems.

$$K = PC^T[CPC^T + R_e]^{-1}. \tag{23}$$

$$P = A(P - PC^T[CPC^T + R_e]^{-1}CP)A^T + R_v, \tag{24}$$

Here, R_e and R_v are covariance matrices of the observation and system noise, respectively. It is assumed that there is no correlation between each observation noise and R_e has white noise following a normal distribution, and R_e is introduced from the variance of the sensor output without any input. Alternatively, R_v is considered as a tuning parameter because the system noise cannot be measured. R_e and R_v are expressed as follows:

$$R_e = \text{diag}(3.86 \cdot 10^{-11}, 1.91 \cdot 10^{-5}, 5.43 \cdot 10^4, 5.09 \cdot 10^4), \tag{25}$$

$$R_v = \text{diag}(10^{-13}, 10^{-7}, 0.5, 1). \tag{26}$$

The measured values of the sensor and the estimated values with the Kalman filter are shown in Fig. 16. In Fig. 16, the responses of z, $\dot{z}$, p_a, and p_b are shown. The solid blue line denotes the measured value, and the dashed line in red denotes the estimated value. z does not have much noise, and the estimated value is almost the same as the measured one. For $\dot{z}$,

p_a, and p_b, there is a delay in the estimated value, but the waveform is mostly the same as the measured one. The true values of responses from 0.5[s] to 1[s] of p_a, and p_b are zero, and the estimated value is accurate, despite the noise in the measured signal. Thus, we confirmed that noise is successively removed. The estimated state variable $\hat{x}[k]$ instead of $x[k]$ is used as measured signal in the experiments, as discussed in the next section. The experiments were conducted successively by removing the noise using the Kalman filter.

6.3. Experimental results

The experimental results (impulse disturbance response) were used to verify the effectiveness of the proposed method. The experimentally obtained impulse disturbance is the same as that in the simulation, and it was applied to system 1 [s] after starting the experiment. In addition, the noise of the air pressure sensor responds sensitively and adds unnecessary inputs before adding the impulse disturbance if $\Delta V[k] < 0$. Therefore, we performed experiments after changing $\Delta V[k] < 0$ to $\Delta V[k] < -1.5 \cdot 10^5$. The designed parameter was introduced as follows:

$$\text{Conventional method} \begin{cases} Q = \text{diag}(4 \times 10^7, 5 \times 10^6, 10^{-6}, 10^{-6}, 10), \\ R = 1, \end{cases} \tag{27}$$

$$\text{Proposed method} \begin{cases} Q = \text{diag}(4 \times 10^4, 2.6 \times 10^6, 10^{-5}, 10^{-5}, 10, 10, 10, 10), \\ R = 1. \end{cases} \tag{28}$$

It is appropriate to use the same parameters, Q and R, for the conventional and proposed methods. However, it is impossible to use the same parameters. This is caused by the same reason described in Section 5.1.2. The experimental results are shown in Figs. 17, 18, and 19. Figures 17 and 18 show the experimental results for both the proposed and conventional methods, and each of the best responses are depicted in Fig. 19. Figs. 17 and 18 were obtained by repeating ten times the same conditions, such as the initial variables, control law, and disturbance. We evaluated the steady-state results to confirm the effectiveness of the proposed method. The RMSE(Root Mean Square Error) and convergence time are shown in Table 1 and Table 2, respectively. Here, the time range of 2 to 4 [s] is employed as the evaluated period for the RMSE, and the convergence time is defined if z converges $|z| < 10^{-4}$ after the impulse disturbance is applied. On the other hand, if z does not converge $|z| < 10^{-4}$, it is expressed as "none". Considering the steady-state error, Figs. 17, 18 and Table 1 show that the proposed method provides superior steady-state error to the conventional method. The difference is attributed to the discrete-valued control as well as the control input resolution. The discrete-valued control law includes dead-band and steady-state error by the multiplicative effect of the dead-band and the integral property of the plant. Superior performance could be obtained in the steady-state if the control input resolution is fine. Thus, the proposed method provides steady-state performance superior to that of the conventional method. For the transient responses, from Figs. 17, 18, 19, and Table 2, the proposed method provides shorter convergence time compared to the conventional method. The input for the conventional method is restricted within 1.5 [s], as shown in Fig. 18, and the trend is the same as that of the simulation results. In contrast, the input for the proposed method is generated after 1.5 [s], as shown in Fig. 17, and it does not coincide with the simulation results. The experimental and simulation output response for the proposed method has almost the same trend, whereas, those for the conventional method show different trends. This means that the proposed method provides superior robust performance compared to the conventional method. The result is attributed to finer control input resolution in the proposed method. Thus, the effectiveness of the proposed method was verified through the experiments.

7. Conclusion

In this study, discrete-valued control systems with discrete actuators are discussed. Specifically, we present examples where control performance decreases during a longer input period and developed a method that improves the control performance. We conducted experiments to verify the proposed method as numerical verifications have already been conducted in (Chida et al., 2019). In addition, a Kalman filter was used to remove noise because the sensor signals were too noisy to properly conduct the experiments. For the above improvement, control experiments were conducted, and the effectiveness of the proposed method was verified by numerical simulations and experiments.
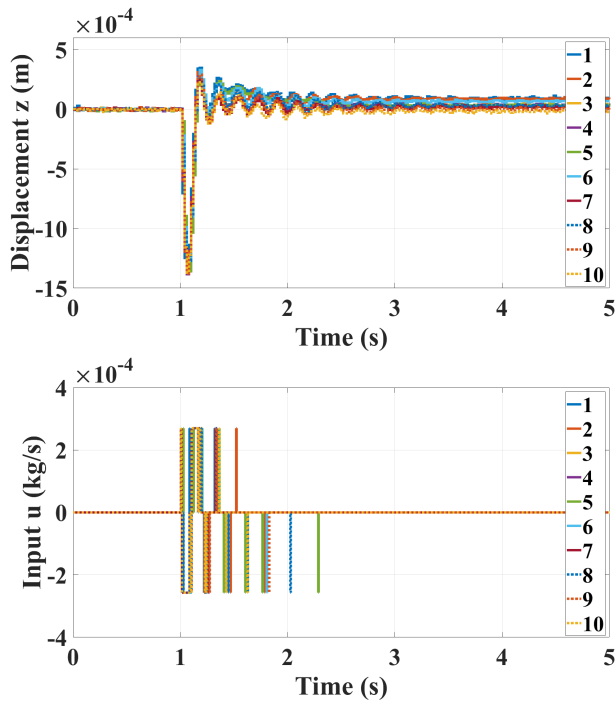
Fig. 17   Experimental results of the proposed method. The experiments are repeated ten times in the same conditions.
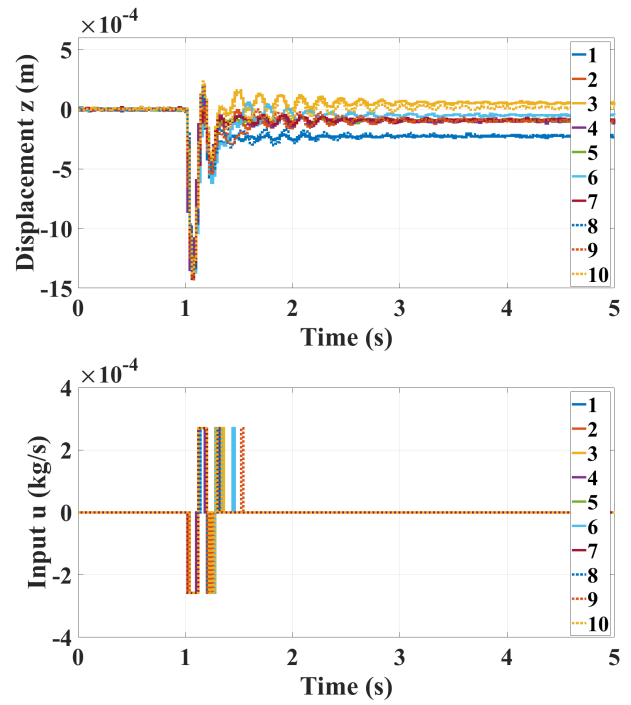

Fig. 18   Experimental results of the conventional method. The experiments are repeated ten times in the same conditions.
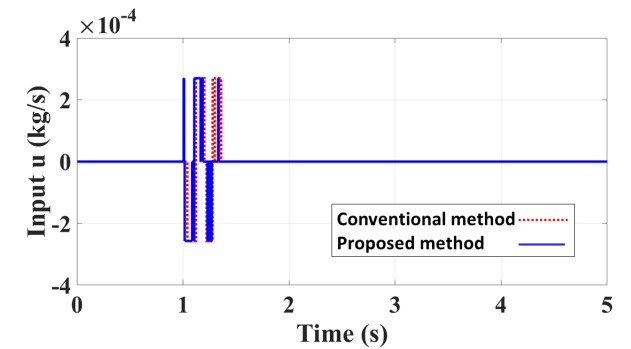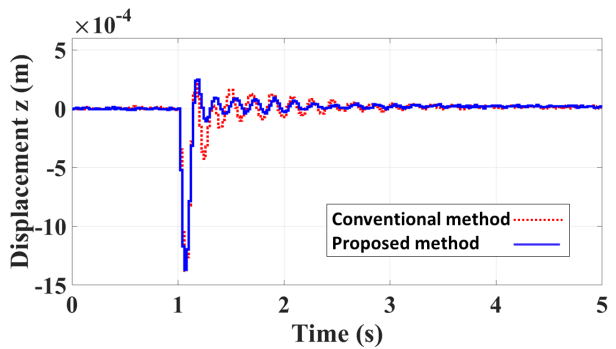

Fig. 19   Experimental results for impulse disturbance response (each best result). The proposed method provides superior performance compared to the conventional method.

Table 1   RMSE of the steady-state error. The proposed method provides smaller errors compared to the conventional method.

	RMSE[m]	
	Proposed method	Conventional method
case1	9.57×10^{-5}	2.29×10^{-4}
case2	8.99×10^{-5}	1.02×10^{-4}
case3	3.97×10^{-5}	5.88×10^{-5}
case4	3.97×10^{-5}	9.89×10^{-5}
case5	4.30×10^{-5}	8.91×10^{-5}
case6	6.65×10^{-5}	5.10×10^{-5}
case7	2.38×10^{-5}	9.03×10^{-5}
case8	4.08×10^{-5}	2.24×10^{-4}
case9	1.67×10^{-5}	9.29×10^{-5}
case10	2.56×10^{-5}	3.16×10^{-5}
average	4.81×10^{-5}	1.07×10^{-4}

Table 2   Convergence time. The proposed method provides rapid convergence time compared to the conventional method.

	Convergence time[s]	
	Proposed method	Conventional method
case1	none	none
case2	none	none
case3	0.940	1.28
case4	0.920	none
case5	0.800	2.66
case6	1.10	0.880
case7	0.280	2.00
case8	1.10	none
case9	0.760	none
case10	0.380	0.920
average	0.785	1.55

References

Azuma, S. and Sugie, T., Synthesis of Optimal Dynamic Quantizers for Symbolic Input Control, Transactions of the Institute of Systems, Control and Information Engineers, Vol. 20, No. 3 (2007), pp. 122-129.(in Japanese)

Azuma, S. and Sugie, T., Synthesis of Optimal Dynamic Quantizers for Discrete-Valued Input Control, IEEE Transactions on Automatic Control, Vol. 53 (2008), pp. 2064-2075.

Berg, M. C., Amit, N. and Powell, J. D., Multirate Digital Control System Design, IEEE Transaction on Automatic Control, Vol. 33, No. 12 (1988), pp. 1139-1150.

Chida, Y., Ishihara, N. and Tanemura, M., Multirate and Model Predictive Control of a Pneumatic Isolation Table with a Discrete Actuator, IFACPapersOnLine, Vol. 52, No. 15 (2019), pp. 442-447.

Dostal, J. and Ferkl, L., Model Predictive Control of Climatic Chamber with On-off Actuators, Proceedings of the 19th World Congress, The International Federation of Automatic Control (2014), pp. 4423-4428.

Fujimoto, H., Application of Multirate Sampling Control to Robot Manipulator, Jounal of the Robotics Society of Japan, Vol. 27 (2009), pp. 410-413.(in Japanese)

Ishikawa, M., Maruta, I. and Sugie, T., Quantized Controller Design Using Feedback Modulators, Transactions of the Society of Instrument and Control Engineers, Vol. 43, No.1(2007), pp. 31-36.(in Japanese)

Koike, M. and Chida.Y, Multivariate Control Design Considering Quantization Error and Input Time-Delay for Pneumatic Isolation Table, Proceedings of ASME 2012 5th Annual Dynamic Systems and Control Conference joint with the JSME 2012 11th Motion and Vibration Conference, Vol. 3 (2012), pp. 783-792.

Koike, M., Chida, Y. and Ikeda, Y., Control of a Pneumatic Isolation Table Including Non-linear Quantizer, Transactions of the Society of Instrument and Control Engineers, Vol. 49, No. 4 (2013), pp. 488-496.(in Japanese)

Maruyama, N., Chida, Y. and Ikeda, Y., Model Predictive Control of Pneumatic Isolation Table with Quantized Input, Proceedings of the SICE Annual Conference (2013), pp. 727-732.

Maruyama, N., Koike, M. and Chida, Y., Model Predictive Control Method for Pneumatic Isolation Table with Discrete-Valued Input, Transactions of the Society of Instrument and Control Engineers, Vol. 51, No. 11 (2015), pp. 755-762.(in Japanese)

Minami, Y., Azuma, S. and Sugie, T., Optimal Dynamic Quantizers in Discrete-Valued Input Feedback Control Systems, Transactions of the Society of Instrument and Control Engineers, Vol. 43, No. 3 (2007), pp. 227-233.(in Japanese)

Mitsuhashi, T., Chida, Y. and Tanemura, M., Autonomous Travel of Lettuce Harvester Using Model Predictive Control, IFACPapersOnLine, Vol. 52, No. 30 (2019), pp. 155-160.

Suzuki, M. and Hirata, M.: Exact linearization of PWM-hold discrete-time systems using input transformation, Proceedings of the European Control Conference (2015), pp. 446-451.